6

A Three-dimensional Continuum Model of Active Contraction in Single Cardiomyocytes

Alessio Gizzi, Ricardo Ruiz-Baier, Simone Rossi, Aymen Laadhari, Christian Cherubini, and Simonetta Filippi

Abstract We investigate the interaction of intracellular calcium spatio-temporal variations with the self-sustained contractions in cardiac myocytes. A 3D continuum mathematical model is presented based on a hyperelastic description of the passive mechanical properties of the cell, combined with an active-strain framework to describe the active shortening of myocytes and its coupling with cytosolic and sarcoplasmic calcium dynamics. Some numerical tests of combined boundary conditions and ionic activations illustrate the ability of our model in reproducing key experimentally established features. Potential applications of the study for predicting pathological subcellular mechanisms affecting e.g. cardiac repolarization are discussed.

6.1 Introduction

Single cells respond to several endogenous and exogenous mechanical stimuli such as stress, strain, strain-rate, strain energy, etc. [24], according to their internal structure. Active cardiac cells, the cardiomyocytes, contain myofibrils bundles in which

A. Gizzi (✉) · C. Cherubini · S. Filippi
Engineering Faculty, University Campus Bio-Medico of Rome, 00128 Rome, Italy
e-mail: a.gizzi@unicampus.it; c.cherubini@unicampus.it; s.filippi@unicampus.it

R. Ruiz-Baier
Institut des Sciences de la Terre, FGSE, Université de Lausanne, 1015 Lausanne, Switzerland
e-mail: ricardo.ruizbaier@unil.ch

S. Rossi
Civil & Environmental Engineering, Mechanical Engineering & Material Science, Duke University, Durham NC, USA
e-mail: simone.rossi@duke.edu

A. Laadhari
Computer Vision Laboratory, ETH Zentrum, CH – 8092 Zurich, Switzerland
e-mail: laadhari@vision.ee.ethz.ch

© Springer International Publishing Switzerland 2015
A. Quarteroni (ed.), *Modeling the Heart and the Circulatory System*,
MS&A 14, DOI 10.1007/978-3-319-05230-4_6

the subcellular contractile units, the sarcomeres, consist of thick and thin interacting myofilaments (myosin and actin proteins, respectively) that generate movement. In the context of muscular tissues, several examples of muscle organizations have been proposed [20,36,45] as the product of a full functional adaptation spanning from the sarcomere length up to the muscle bundle [53].

The excitation-contraction mechanism in these media is usually coordinated by an external electrical activation and propagated through specialized networks, the Purkinje fibers, to the whole tissue [29].

At the microscale, calcium ions (Ca^{2+}) flow through the cell membrane from the extracellular matrix and are exchanged between the cytosol and sarcoplasmic reticulum thus regulating the interaction of the myofilaments. This chemical process onsets the shortening of the sarcomeres and drives the excitation-contraction coupling of the whole cardiac cell. The Calcium-Induced Calcium Released (CICR) feedback, in particular, originates in the excited state when the sarcolemma gets depolarized inducing the influx of extracellular calcium into the cardiomyocytes; the increase of intracellular calcium induces more Ca^{2+} to be released from the sarcoplasmic reticulum; cytosolic Ca^{2+} ions bind to troponin-C and activate the myofilaments. The process ends when the cell gets depolarized thus reducing the level of calcium concentration via both outflow fluxes and calcium sequestration in the sarcoplasmic reticulum. Although the excitation-contraction mechanism and the CICR feedback have major evidences both at the theoretical [56] and experimental [12] levels, the full understanding of the exact interplay between the different processes involved is still lacking. Nonetheless, these subcellular mechanisms play a key role in the overall cardiac function. Their understanding can therefore be of utmost importance and interest for the study of many physiological and pathological conditions [2,22].

Different systemic effects of cardiac mechano-electric interactions can be explored by studying the elastic properties of isolated cardiac myocytes [21,26,37,53]. Experimental evidences have shown that stress concentrations can often be recorded at locations without visible fibers deformations [10]. Such a phenomenon motivates the hypothesis that stresses are induced by micro-structure remodeling acting on a much smaller scale than the cell one and justifies the choice of a contractility model formulated at the continuum level. This allows to characterize a multiscale process rather than the description of an ensemble of particles by assuming: (i) a sufficient level of calcium concentration without limiting the mechanical activation; (ii) a representative volume element (RVE) inside the cell can be identified; and (iii) a mechanical response can be observed from any direction.

In this contribution we provide a quantitative description of the behavior of a single myocyte by proposing a complete chemo-active-mechanical model for three-dimensional cell geometries under specified experimental conditions and in agreement with the current mechanobiology approach [58]. Ionic kinetics and voltage-dependent equations at the cellular level are carefully considered [46]. Due to the complexity of the problem at hand, we focus our numerical simulations on describing the behavior of the principal calcium concentrations inside the cardiomyocyte and their nonlinear interplay with the mechanical quantities. Specific applications in the cardiovascular context analyzing boundary constraints, e.g. cell-cell and cell-matrix

adhesion, are discussed in terms of a positive feedback loop towards the functional organization and stress level on the cell membrane [21,37].

The mathematical model here proposed is based on the active-strain approach [39, 51] in which the mechanical activation is formulated as a *virtual* multiplicative decomposition of the deformation gradient into a passive elastic response and an active deformation contribution. The latter is directly coupled to a simplified nonlinear model of calcium dynamics [19, 54, 61]; this allows us to consider both the anisotropic passive intracellular organization, i.e. the T-tubule system, and the anisotropic active emerging cellular structures.

The generalized formulation is thermodynamically consistent [17,50,55] and allows the characterization of the interactions among ionic quantities, cellular mechanical properties and environmental effects. In particular, it explains the influence of cell shape and boundary conditions on the onset of structural anisotropies and stress concentrations. We address all of these requirements with the aid of finite-element-based simulations characterizing the feasibility and adequateness of employing a macroscopic description of the mechano-chemical behavior of a single cell. Such a modeling strategy, moreover, is well suited to explain the complex relations between microscopic cell dynamics and macroscopic cardiac functions. Three-dimensional simulations in this direction will be discussed. Our model is myocyte bending-contraction dynamics and end terminals deformations.

6.2 Continuum Model for Single Cell Biomechanics

Let $\mathbf{x}$ represent the current position of a material particle of the myocyte Ω_t, that occupied the position $\mathbf{X}$ in the natural stress-free configuration $\Omega_0 \subset \mathbb{R}^3$ with boundary Γ_0. Motion can be expressed in terms of the displacement vector field $\mathbf{d} = \mathbf{x} - \mathbf{X}$, and as usual, we denote by $\mathbf{F} = \nabla_{\mathbf{X}}\mathbf{x}$, $\mathbf{C} = \mathbf{F}^T\mathbf{F}$ and $\mathbf{B} = \mathbf{F}\mathbf{F}^T$ the deformation gradient tensor and the right, left Cauchy-Green deformation tensors, respectively, where ∇ is the gradient with respect to material coordinates.

In a general form, the passive mechanical response of an isolated cell can be described through a hyperelastic, anisotropic constitutive law derived from the one proposed in [23] to model tissue properties, here written for a quasi-incompressible material:

$$\begin{aligned}\mathscr{W}(\mathbf{F}) = \frac{a}{2b}\left[\exp(b[\overline{I}_1 - 3]) - 1\right] + \frac{a_f}{2b_f}\left[\exp(b_f[\overline{I}_{4,f} - 1]^2) - 1\right] \\ + \frac{\kappa}{4}\left[(J-1)^2 + (\ln J)^2\right],\end{aligned} \tag{6.1}$$

where a is a shear modulus, κ a bulk modulus, a_f, b, b_f are experimentally fitted in order to recover the strain-stress relationships found in [61] employing a polynomial strain energy function (see Fig. 6.1 and Table 6.1), and $\overline{I}_1 := J^{-2/3}\,\mathrm{tr}(\mathbf{C})$, $\overline{I}_{4,f} := J^{-2/3}\mathbf{F}\mathbf{f}_0 \cdot \mathbf{F}\mathbf{f}_0$, are isotropic and direction-dependent invariants. Here $\mathbf{f}_0$ is a unitary direction vector in the reference configuration representing the myofibrils alignment.

Table 6.1. Parameters for passive mechanical anisotropic response on a single cell

Transversely isotropic passive response				
$a = 3.2639$ kPa	$a_f = 0.1354$	$b = 2.7492$ kPa	$b_f = 5.4536$	$\kappa = 350$ kPa

The governing equations of motion are set in the reference configuration and are endowed with Robin boundary conditions:

$$\begin{aligned} \rho\partial_{tt}\mathbf{d} - \nabla\cdot\mathbf{P} &= \rho\mathbf{b} \quad \text{in } \Omega_0\times(0,T), \\ \mathbf{P}\nu + \alpha_R\mathbf{d} &= \mathbf{d}_0 \quad \text{on } \Gamma_0\times(0,T), \end{aligned} \tag{6.2}$$

where $\mathbf{b}$ is a body force per unit mass, ν is the unit normal vector to the cell on Γ_0, $\mathbf{d}_0$ is a prescribed boundary load, α_R is a Robin coefficient, ρ is the referential mass density, and the (first Piola-Kirchhoff) stress tensor associated to (6.1) is specified as

$$\begin{aligned} \mathbf{P} = {} & a\exp(b[I_1-3])J^{-2/3}\left(\mathbf{F} - \frac{I_1}{3}\mathbf{F}^{-T}\right) \\ & + 2a_f(I_{4,f}-1)\exp(b_f[I_{4,f}-1]^2)J^{-2/3}\left(\mathbf{F}\mathbf{f}_0\otimes\mathbf{f}_0 - \frac{I_1}{3}\mathbf{F}^{-T}\right) \\ & + \frac{\kappa}{2}\left(J^2 - J + \ln J\right)\mathbf{F}^{-T}. \end{aligned}$$

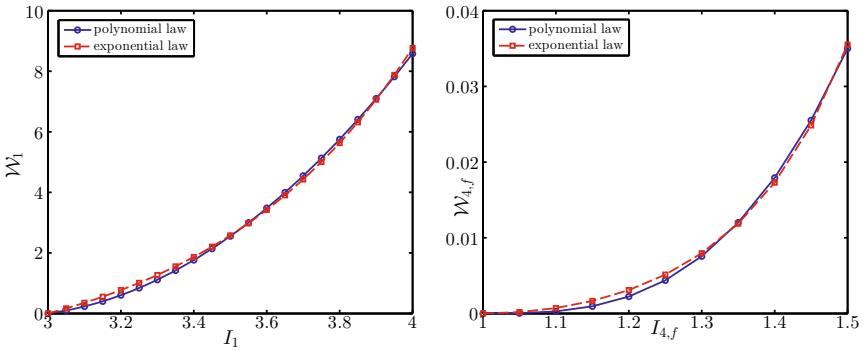

Fig. 6.1. Fitting of the transversely isotropic strain energy (6.1) with respect to the polynomial energy function proposed in [61]. Here $\mathcal{W}_1 = \frac{a}{2b}[\exp(b[I_1-3])-1]$ and $\mathcal{W}_{4,f} = \frac{a_f}{2b_f}\left[\exp(b_f[I_{4,f}-1]^2)-1\right]$. The obtained parameters are displayed in Table 6.1

6.3 Intracellular Ionic Dynamics

This section briefly introduces the model equations of the phenomenological cardiac action potential propagation [6] and of the CICR calcium dynamics [19] for deformable anisotropic media.

6.3.1 Minimal Model

The four-variable minimal phenomenological model for cardiac action potential propagation [5] allows us to quantify the key parameters necessary to correctly reproduce the experimental restitution properties (see also [15]) within minimal levels of computational requirements. Other effects can be recovered with significantly more complex ionic models [14]. Using the monodomain description for cardiac electrophysiology, the model equations are given by:

$$\begin{aligned}
C_m\chi_m\partial_t u &= \nabla\cdot(\mathbf{D}\nabla u) - \chi_m\left(J_{fi}+J_{so}+J_{si}\right) && \text{in } \Omega_0\times(0,T),\\
\partial_t v &= [1-H(u-\theta_v)]v_\infty - v/\tau_v^- - H(u-\theta_v)v/\tau_v^+ && \text{in } \Omega_0\times(0,T),\\
\partial_t w &= [1-H(u-\theta_w)](w_\infty - w)/\tau_w^- - H(u-\theta_w)w/\tau_w^+ && \text{in } \Omega_0\times(0,T),\\
\partial_t s &= \left(1+\tanh[k_s(u-u_s)]\right)/2\tau_s - s/\tau_s && \text{in } \Omega_0\times(0,T),\\
(\mathbf{D}\nabla u)\cdot\nu &= 0 && \text{on } \Gamma_0\times(0,T),
\end{aligned} \tag{6.3}$$

where C_m is the specific membrane capacitance per unit area, χ_m is the surface-to-volume ratio of the cell, and $\mathbf{D}=\mathbf{F}^{-1}\,\mathrm{diag}(D_f,D_s,D_n)\mathbf{F}^{-T}$ is a tensor of tissue conductivities D_f, D_s, D_n. The ionic density currents are defined as

$$J_{fi} = -H(u-\theta_v)(u-\theta_v)(u_u-u)\frac{v}{\tau_{fi}},$$
$$J_{so} = [1-H(u-\theta_w)]\frac{u-u_o}{\tau_o} + \frac{H(u-\theta_w)}{\tau_{so}}, \quad J_{si} = -H(u-\theta_w)\frac{ws}{\tau_{si}},$$

and refer to a fast inward, J_{fi}, a slow outward, J_{so}, and a slow inward, J_{si}, flux, respectively. Other than fixed time constants, the model is equipped by the following voltage-dependent time constants

$$\begin{aligned}
\tau_v^-(u) &= [1-H(u-\theta_v^-)]\tau_{v1}^- + H(u-\theta_v^-)\tau_{v2}^-,\\
\tau_w^-(u) &= \tau_{w1}^- + (\tau_{w2}^- - \tau_{w1}^-)\{\tanh(k_w^-[u-u_w^-)]+1\}/2,\\
\tau_{so}(u) &= \tau_{so1} + (\tau_{so2}-\tau_{so1})\{\tanh[k_{so}(u-u_{so})]+1\}/2,\\
\tau_s(u) &= [1-H(u-\theta_w)]\tau_{s1} + H(u-\theta_w)\tau_{s2},\\
\tau_o(u) &= [1-H(u-\theta_o)]\tau_{o1} + H(u-\theta_o)\tau_{o2}\,.
\end{aligned}$$

Here $H(\cdot)$ is the Heaviside step function; u is the dimensionless membrane potential rescaled to physical dimensions by using the map $V_m=(85.7u-84)\,mV$; v, w and s

Table 6.2. Parameters for ionic activity according to the minimal and Goldbeter models (units are given in *ms*, *cm*, *mV*, *mS*, μF, *g*, $k\Omega^{-1}\mathrm{cm}^{-1}$)

Minimal model
$u_o = 0$, $u_u = 1.55$, $\theta_v = 0.3$, $\theta_w = 0.13$, $\theta_v^- = 0.006$, $\theta_o = 0.006$,
$\tau_v^+ = 1.4506$, $\tau_{v1}^- = 20$, $\tau_{v2}^- = 1150$, $\tau_{w1}^- = 120$, $\tau_{w2}^- = 300$, $\tau_{w1}^+ = 120$, $\tau_{w2}^+ = 140$,
$k_w^- = 65$, $u_w^- = 0.03$, $k_w^+ = 5.7$, $u_w^+ = 0.15$, $\tau_{fi} = 0.11$ $\tau_{o1} = 400$, $\tau_{o2} = 6$,
$\tau_{so1} = 30.0181$, $\tau_{so2} = 0.9957$, $k_{so} = 2.0458$, $u_{so} = 0.65$, $\tau_{s1} = 2.7342$, $\tau_{s2} = 16$,
$k_s = 2.0994$, $u_s = 0.9087$, $\tau_{si} = 1.8875$, $\tau_{w\infty} = 0.07$, $w_\infty^* = 0.94$,
$D_f = 1.33417721$, $D_s = 0.17606$, $D_n = 0.17606$, $C_m = 1$, $\chi_m = 1400$
Goldbeter model
$\alpha = 0.01$, $a = 0.496$, $\nu_1 = 1.58$, $\nu_2 = 16$, $\nu_3 = 91$, $\nu_4 = 2$, $\nu_5 = 1$,
$k_2 = 4$, $k_3 = 0.7481$, $D_f = 60$, $D_s = 30$, $D_n = 30$

are the three local gating variables, and the asymptotic values are given by

$$v_\infty = \begin{cases} 1, & u < \theta_v^- \\ 0, & u \geq \theta_v^- \end{cases}, \quad w_\infty = [1 - H(u-\theta_o)]\left(1 - \frac{u}{\tau_{w\infty}}\right) + H(u-\theta_o)w_\infty^*.$$

Model parameters are reported in Table 6.2.

6.3.2 Goldbeter Model

In experiments on skinned isolated ventricular myocytes, or when the sarcolemma is hyper-permeable to calcium [3, 13], spontaneous contractile waves have been observed. These waves are related to slow calcium propagation ($\sim$100 μm/s) driven by the spontaneous release of calcium from the sarcoplasmic reticulum [60]. While these waves are not physiological (they do not develop during physiological pacing [6]), their occurrence during normal stimulation can be regarded as pathological and may give rise to arrhythmic scenarios [62]. The study of intracellular calcium wave propagation requires a model tuned to recover slow diffusion of $[Ca^{2+}]$, coupled to CICR, from channels sensitive to ryanodine release in the sarcoplasmic reticulum [57]. Here we focus on the following system of partial differential equations governing simplified CICR dynamics [19]:

$$\begin{aligned} \partial_t w_c &= \nabla \cdot (\mathbf{D}\nabla w_c) + K(w_c, w_s) && \text{in } \Omega_0 \times (0,T), \\ \partial_t w_s &= L(w_c, w_s) && \text{in } \Omega_0 \times (0,T), \\ (\mathbf{D}\nabla w_c) \cdot \nu &= 0 && \text{on } \Gamma_0 \times (0,T), \end{aligned} \tag{6.4}$$

where w_c and w_s represent the concentrations of cytosolic and sarcoplasmic calcium, respectively. Only two calcium species are considered under the assumption that the level of IP_3 (responsible for the increase in the intracellular calcium concentration) remains constant during external stimulation. Anisotropy of the cell is accounted by

the form of the diffusion tensor $\mathbf{D} = J\mathbf{F}^{-1}\,\mathrm{diag}(D_f, D_s, D_n)\mathbf{F}^{-T}$, where D_f, D_s, D_n are diffusivities of cytosolic calcium in three orthogonal directions, and the reaction terms are

$$K(w_c, w_s) = \nu_1 - \frac{\nu_2 w_c^2}{k_2 + w_c^2} + \frac{\nu_3 w_c^4 w_s^2}{(k_3 + w_s^2)(k_4 + w_c^4)} - \nu_4 w_c,$$

$$L(w_c, w_s) = \frac{\nu_2 w_c^2}{k_2 + w_c^2} - \frac{\nu_3 w_c^4 w_s^2}{(k_3 + w_s^2)(k_4 + w_c^4)} - \nu_5 w_s,$$

with ν_1 representing an inflow flux plus intracellular calcium pulses originated from the asynchrony of calcium pools receptors, ν_2 and ν_3 accounting for low and high levels of free cytosolic calcium flux pumped from the sarcoplasmic reticulum, and ν_4 modeling an efflux of calcium out of the cell following a chemical exchange process (see also e.g. [61]). Model parameters are displayed in Table 6.2.

6.4 A Mathematical Model for Mechanical Activation

Our description follows the active strain approach [8,38,50], where the deformation gradient is split into a passive and an active component, $\mathbf{F} = \mathbf{F}_\mathrm{P}\mathbf{F}_\mathrm{A}$, implying that a passive (say, purely elastic) intermediate configuration exists between the reference and the deformed one (see Fig. 6.2). Such a multiplicative decomposition of the deformation gradient is typical in many constitutive theories in finite kinematics (see e.g. [32,42–44,63]), and it has been shown to yield computational efficiency in numerical applications.

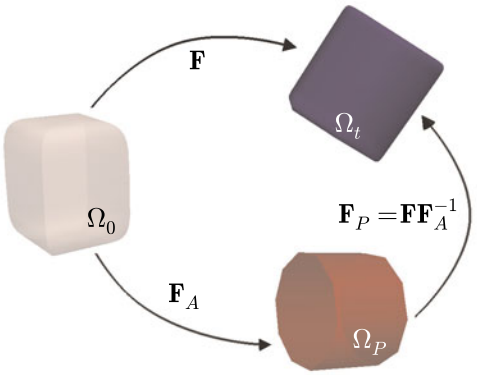

Fig. 6.2. Schematic representation of the active strain framework leading to the decomposition of the deformation gradient into a pure active and an elastic (passive) factor. Here $\Omega_0, \Omega_P, \Omega_t$ represent a body in its reference, incompatible intermediate, and deformed configuration, respectively

The tensor $\mathbf{F}_{\mathrm{A}}$ represents the intermediate motion and describes the active deformations of the cell. It can be written in the general form

$$\mathbf{F}_{\mathrm{A}} = \mathbf{I} + \gamma_{\mathrm{f}} \mathbf{f}_0 \otimes \mathbf{f}_0 + \gamma_{\mathrm{s}} \mathbf{s}_0 \otimes \mathbf{s}_0 + \gamma_{\mathrm{n}} \mathbf{n}_0 \otimes \mathbf{n}_0,$$

where γ_{f}, γ_{s} and γ_{n} are smooth scalar functions encoding the active shortening of the cardiomyocytes and their corresponding thickening [25]. If we define $\mathbf{C}_{\mathrm{A}} = \mathbf{F}_{\mathrm{A}}^T \mathbf{F}_{\mathrm{A}}$, $\mathbf{F}_{\mathrm{P}} = \mathbf{F}\mathbf{F}_{\mathrm{A}}^{-1}$, $\mathbf{C}_{\mathrm{P}} = \mathbf{F}_{\mathrm{A}}^{-T}\mathbf{C}\mathbf{F}_{\mathrm{A}}^{-1}$, $J_A = \det \mathbf{F}_{\mathrm{A}}$, $J_P = \det \mathbf{F}_{\mathrm{P}}$, $J = J_P J_A$, then the strain energy (6.1) can be rewritten in the intermediate configuration Ω_P, now in terms of $\mathbf{F}_{\mathrm{P}}$ and as a function of the following quantities

$$\overline{I}_1^{\mathrm{P}} := \overline{I}_1 - \sum_{l \in \{f,s,n\}} \frac{\gamma_{\mathrm{l}}(\gamma_{\mathrm{l}}+2)}{(\gamma_{\mathrm{l}}+1)^2} \mathbf{F}\mathbf{l}_0 \cdot \mathbf{F}\mathbf{l}_0, \quad \overline{I}_{4,f}^{\mathrm{P}} := (1+\gamma_{\mathrm{f}})^{-2} \overline{I}_{4,f},$$
$$\psi_1^{\mathrm{P}} := \frac{a}{2} \exp(b[\overline{I}_1^{\mathrm{P}} - 3]), \quad \psi_{4,f}^{\mathrm{P}} := a_f(\overline{I}_{4,f}^{\mathrm{P}} - 1)\exp(b_f[\overline{I}_{4,f}^{\mathrm{P}} - 1]^2).$$

Even if the isolated myocyte is not a closed system in equilibrium, energy dissipation, achieved by means of internal state variables, allows us to derive an evolution law for the mechanical activation field γ_f. The multiplicative decomposition of the deformation gradient suggests that the active deformation gradient tensor can be regarded as the internal state variable describing mechanical activation [50]. In practice we consider a free energy ψ additively decomposed as

$$\psi(\mathbf{F}_E, \mathbf{c}) = \psi(\mathbf{F}, \mathbf{F}_A, \mathbf{c}) = \psi_P(\mathbf{F}) + \psi_A(\mathbf{F}, \mathbf{F}_A) + \psi_C(\mathbf{c}),$$

where $\mathbf{c}$ is a vector containing all the chemical species involved in the myocyte contraction. We suppose that there exists a microstructural stress $\mathbf{P}_A$ yielding the microstructural stress power $\mathbf{P}_A : \dot{\mathbf{F}}_A$. The active stress $\mathbf{P}_A$ is a function of subcellular chemical quantities encoded in the vector $\mathbf{c}$. By means of the generalized dissipation inequality, using the Coleman-Noll procedure we obtain

$$\left(\mathbf{P} - \frac{\partial \psi_P}{\partial \mathbf{F}} - \frac{\partial \psi_A}{\partial \mathbf{F}}\right) : \dot{\mathbf{F}} + \left(\mathbf{P}_A - \frac{\partial \psi_A}{\partial \mathbf{F}_A}\right) : \dot{\mathbf{F}}_A - \frac{\partial \psi_C}{\partial \mathbf{c}} \dot{\mathbf{c}} \geq 0.$$

The quantity $\frac{\partial \psi_A}{\partial \mathbf{F}_A}$ represents the configurational forces associated with $\mathbf{F}_A$. This relation holds in particular for

$$\mathbf{P} = \frac{\partial \psi_P}{\partial \mathbf{F}} + \frac{\partial \psi_A}{\partial \mathbf{F}},$$
$$\mu_A \dot{\mathbf{F}}_A = \mathbf{P}_A(\mathbf{c}) - \frac{\partial \psi_A}{\partial \mathbf{F}_A},$$
$$0 \leq \frac{\partial \psi_C}{\partial \mathbf{c}} \cdot \dot{\mathbf{c}}.$$

We consider an orthotropic stress tensor incorporating an active contribution

$$\mathbf{P} = 2\psi_1^{\mathrm{P}} J^{-2/3}\left[(1+\gamma_f)^2\mathbf{F} - g(\gamma_f)\mathbf{F}\mathbf{f}_0\otimes\mathbf{f}_0 - \frac{I_1^P}{3}\mathbf{F}^{-T}\right] - \frac{\kappa}{2}\left(J^2 - J + \ln J\right)\mathbf{F}^{-T}$$
$$+ 2\psi_{4,f}^P\left[\frac{1}{\left(1+\gamma_f\right)^2}\mathbf{F}\mathbf{f}_0\otimes\mathbf{f}_0 - \frac{I_{4,f}^P}{3}\mathbf{F}^{-T}\right], \tag{6.5}$$

where $g(\gamma_{\mathrm{f}}) = \gamma_{\mathrm{f}} + \gamma_{\mathrm{f}}\frac{\gamma_{\mathrm{f}}+2}{(1+\gamma_{\mathrm{f}})^2}$. We consider the activation dynamics to be given as in [51] by the relation

$$\partial_t\gamma_{\mathrm{f}} = \beta^{-1}\left(P_A - [2(1+\gamma_{\mathrm{f}})I_1 + g'(\gamma_{\mathrm{f}})I_{4,f}]\psi_1^{\mathrm{P}} - \frac{2}{(1+\gamma_{\mathrm{f}})^3}I_{4,f}\psi_{4,f}^{\mathrm{P}}\right) \quad \text{in } \Omega_0\times(0,T), \tag{6.6}$$

where P_A is fitted from data and β is a function of calcium concentration, provided by either s from the minimal model, or w_c from the Goldbeter model. For more details we refer to [50, 51].

The final set of equations describing the mechano-chemical coupling in a single cell are given by the nonlinear elasticity problem (6.2) with $\rho = 0$ and $\mathbf{P}$ as in (6.5), the activation dynamics (6.6), and the ionic activity governed by either (6.3) or (6.4).

6.5 Discretization and Numerical Examples

The spatial segregation of cell-matrix and cell-cell adhesions to individual myocyte borders has important effects for the electromechanical coupling within the tissue as well as for the onset of electrical arrhythmias [33]. Such adhesions consist of localized boundary conditions anchoring cells and tissues to the extracellular matrix. From the biomechanical point of view, moreover, these specialized boundaries are mechanosensitive and can act as tunable constraints locally modifying the stress concentration according to the cell function or modulating tissue organization as well. Recently, cell membrane boundary condition effects on cardiomyopathies have been experimentally characterized by increased fibrosis and tissue stiffening [1, 18] via a fine characterization of the interaction between cells and stiff substrates. These complex feedbacks and focal adhesions, moreover, play an important role in the organization of cytoskeletal scaffolds, stabilizing the mechanical response of the myocyte, their structure and function as well as their resulting contractile response [9, 21, 37].

In the following sections we present numerical examples in this direction by comparing different boundary conditions and activation processes on a realistic three-dimensional myocyte geometry. Domain segmentation, mesh generation and FEM implementation are described.

6.5.1 Geometry Segmentation and Mesh Generation

A three-dimensional computational domain was obtained with image segmentation tools applied to a canine cardiomyocyte [4] (employing a Zeiss LSM-510 META

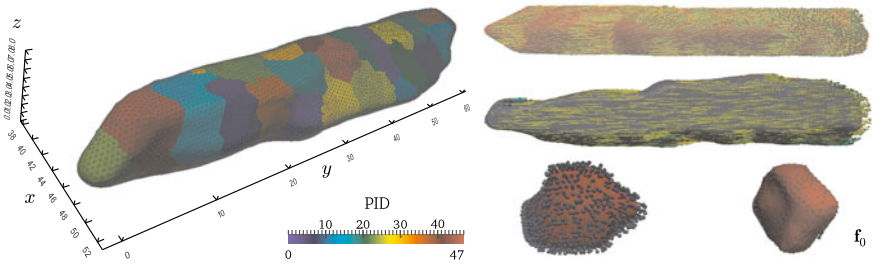

Fig. 6.3. Cell geometry, subdomain partitions and tetrahedral mesh (*left*), and lateral, aerial, back and front views of the constructed fibers field (*right*). In the text we mention "left" and "right" ends of the cell referring to the endpoints at $y = -1.7\,\mu$m and $y = 61.2\,\mu$m, respectively

confocal microscope). The starting images were in a stress-free/strain-free configuration and the cell has approximate dimensions of $15.3\mu\text{m} \times 62.9\mu\text{m} \times 8\mu\text{m}$. An in-house code based on MATLAB and COMSOL Multiphysics interface was used to discretize the surface geometry into an initial triangular mesh that merged the set of confocal cell image slices. Such initial surface mesh exhibits several irregularities (e.g. holes, boundary edges, flipped triangles and poor quality edges) which, in particular, violate the correct cell shape. These issues were solved using Meshlab (meshlab.sourceforge.net): we removed self intersecting faces and non-manifold faces, and we applied several local smoothing and remeshing steps in order to obtain a well-resolved boundary. Additional mesh optimization (faces regularity and so on) along with volumetric mesh generation was performed in Gmsh [16]. The final mesh consists of 77031 tetrahedral elements and 18191 vertices (see Fig. 6.3, left).

A preferred direction field for the mechanical activation within the myocyte (here denoted with $\mathbf{f}_0$) basically corresponds to the sarcomeres orientation (see e.g. [61]). We generated such a direction field using a general rule-based method detailed in [50] for fibers and sheets directions in ventricular tissue. The algorithm uses a Laplace-Dirichlet approach. Once boundaries patches on the "top" and "bottom" of the cell are defined, we solve a diffusion problem imposing homogeneous Dirichlet conditions on these boundaries. The resulting preferred direction of anisotropy is oriented according to the direction of diffusion gradient (see Fig. 6.3, right).

6.5.2 Finite Element Approximation

The equations of nonlinear elasticity and the reaction-diffusion systems for ionic activity and mechanical activation are discretized in space by $\mathbb{P}_2$ and $\mathbb{P}_1$, respectively. The solution of the coupling employs a modular approach, which allows us in particular to use different time steps for the elasticity and reaction-diffusion solvers. All other nonlinearities are treated with a nonlinear Richardson method and the time discretization of the coupled problem is as follows. An operator-splitting scheme is employed for the solution of the electrophysiology (or alternatively calcium) equa-

tions. The diffusion part is discretized in time using the implicit Euler method and the system of equations is solved using the conjugate gradient method with an algebraic multigrid preconditioner using 4 levels computed by smoothed aggregation, where the pre- and post-smoother at each level is two sweeps of Gauss-Seidel iteration, and at the coarse level we take two sweeps of the conjugate gradient method. Further details can be found in [50].

Code implementation has been carried out in the framework of the open source finite element library LifeV (www.lifev.org). All simulations were performed on four cluster nodes with two Sandy Bridge processors (8 core, 2.2 GHz CPU) each, representing a total of 64 CPUs using Infiniband QDR 2:1 connectivity (hpc.epfl.ch/clusters/bellatrix).

6.5.3 Example 1: Single Cell Electromechanics

Under physiological conditions a single myocyte is excited almost instantaneously. In fact, considering a conduction velocity of about 70 cm/s for the electrical signal, a cell with an approximate length of 100 μm is fully electrically activated in about 0.1 ms. In this way the subcellular contraction mechanism is initiated almost simultaneously in all regions of the cell. These circumstances allow us to test the proposed activation model on simplified yet significant cases. The monodomain equation describes the transmembrane potential and therefore cannot be applied in the whole cell. On the other hand, by the considerations above, there is no need to consider electrical propagation. By solving the ionic model alone, we can extend the calcium-like variable s in the whole intracellular space allowing the triggering of the mechanical activation model and cellular contraction. In Fig. 6.4 (left) we recall the evolution of the minimal model and the calcium-like variables. The gating variable s is used in the activation model in place of intracellular calcium concentration, not available in the minimal model. The computed evolution of the active strain is also shown in

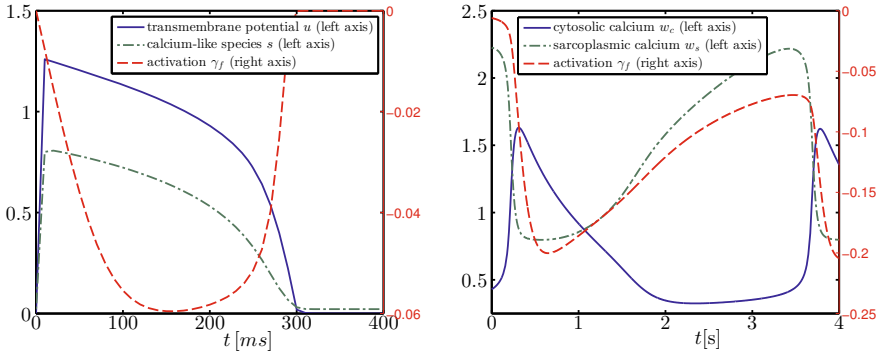

Fig. 6.4. Examples 1 and 2: Dynamics of voltage, calcium concentration, and activation measured on a single point near the cell center, through time for the minimal and Goldbeter models (*left and right panels*, respectively)

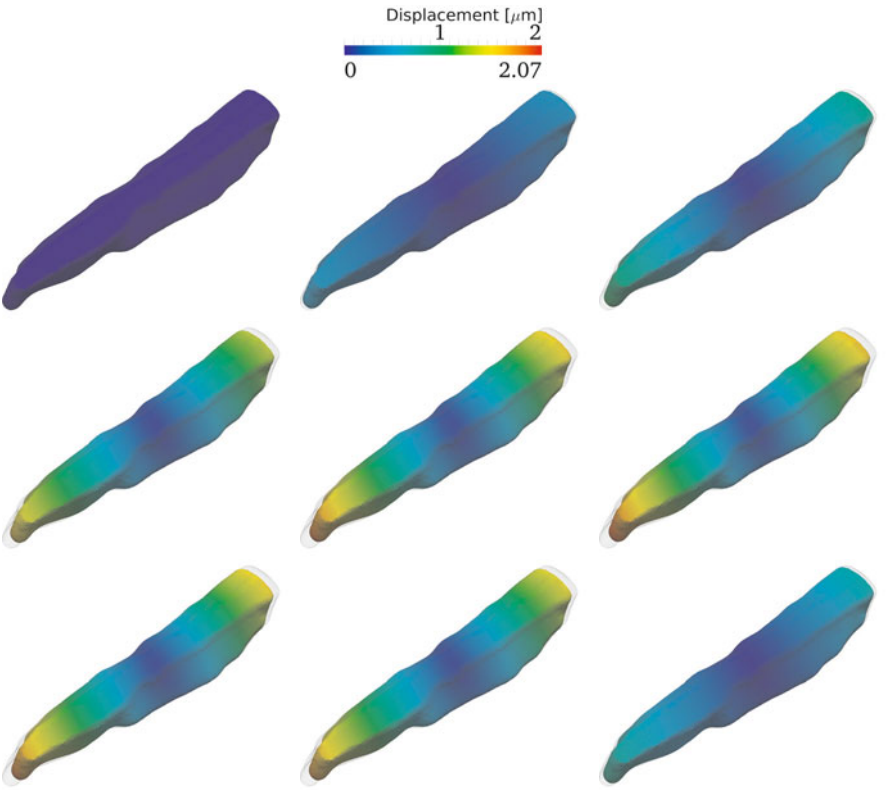

Fig. 6.5. Example 1: Displacement field and deformed domain for times $t = 0$, 20, 40, 80, 120, 180, 220, 240, 280 ms

Fig. 6.4 (left). Given the specific kinetics of species s, more prolonged with respect to intracellular calcium concentration, the active strain γ_f is able to represent cellular contraction.

Since pure stress-free boundary conditions do not eliminate possible rigid motion, we set Robin boundary conditions as in (6.2), with $\mathbf{d}_0 = \mathbf{0}$ and $\alpha_R = 50\,\mathrm{Pa/m}$ on the left and right ends of the cell, and we put $\alpha_R = 10\,\mathrm{Pa/m}$ elsewhere in Γ_0. In this way the cell shortens symmetrically by about 6% of its resting length as shown in Fig. 6.5, in accordance with other cellular models [48, 64].

6.5.4 Example 2: Intracellular Calcium Transients

We now turn to the simulation of slow calcium waves inside the cell. Self-sustained mechano-chemical interactions are initiated by a single cytosolic calcium spark near the nucleus of the cell (as in e.g. [26, 61]). The kinetics of a single point near the cell center are plotted in Fig. 6.4 (right). We test Robin and Dirichlet boundary con-

ditions simulating adhesion regions, or alternatively the contact with surrounding myocytes. In Figs. 6.6 and 6.7 we observe the propagation of w_c towards the extremities of the cell comparing the two sets of boundary conditions: the displacements are constrained to Robin data on the whole boundary (Fig. 6.7) and fixed to zero the left end of the cell and stress-free elsewhere (Fig. 6.6). As predicted in our previous 2D tests (see [51]) we here observe cell bending in the first case, whereas for spring

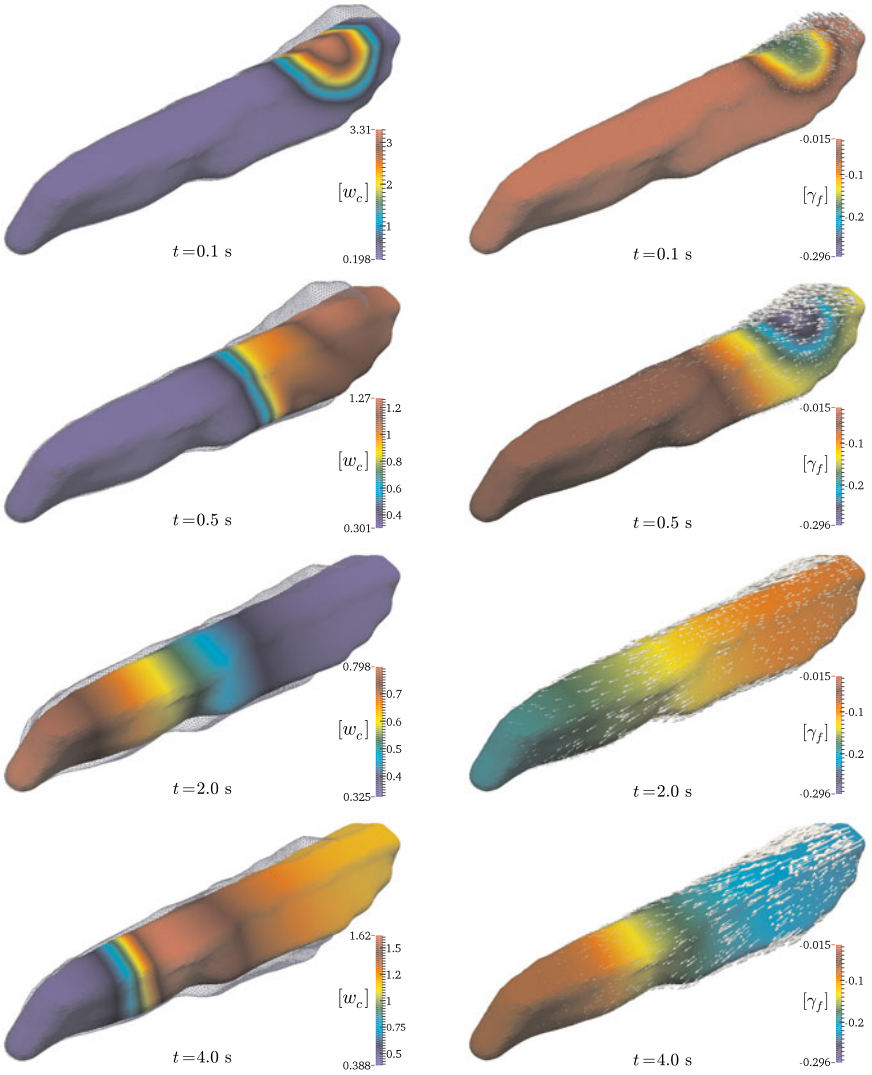

Fig. 6.6. Example 2: Snapshots of the propagation of cytosolic calcium and deformed domain (*left panels*) and activation function γ_f with displacement vectors (*right panels*) for times $t = 0.1, 0.5, 2.0, 4.0$s (*from top to bottom*) when the cell is fixed on the left end

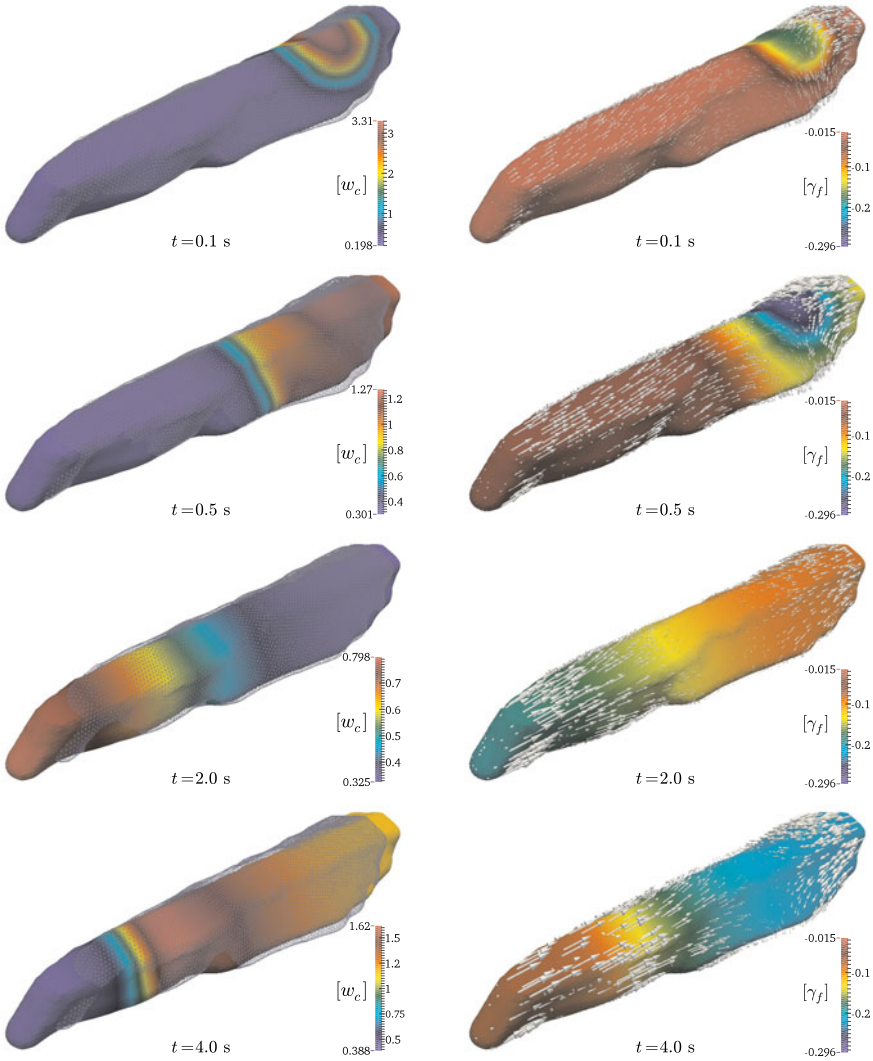

Fig. 6.7. Example 2: Snapshots of the propagation of cytosolic calcium and deformed domain (*left panels*) and activation function γ_f with displacement vectors (*right panels*) for times $t = 0.1, 0.5, 2.0, 4.0$ s (*from top to bottom*) for pure Robin boundary data

boundary data the contraction patterns are symmetric with respect to the cell center. Movement with respect to the principal direction $\mathbf{f}_0$ and bending are expected in realistic scenarios [9]. Finally we compare our cases with the study reported in [28] in terms of contractility patterns of the cell ends (see also [31]). Our results (for pure Robin boundary data) show a reasonable qualitative agreement, considering that the cell shapes do not coincide (see Fig. 6.8).

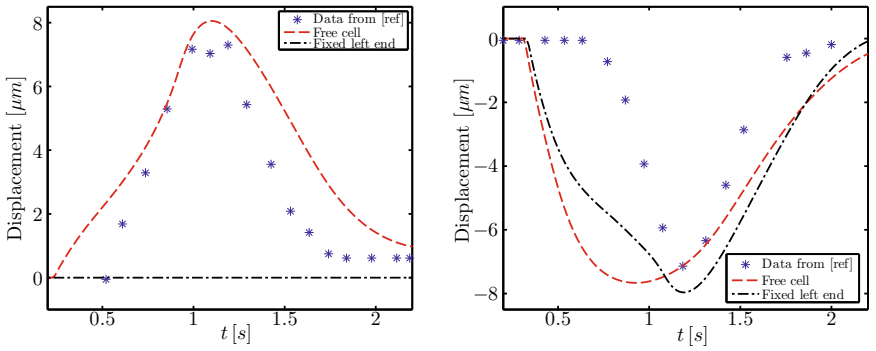

Fig. 6.8. Example 2: Cell contraction dynamics measured by displacements on the left and right ends of the myocyte (*left and right panels*, respectively) and comparison with respect to experimental observations from [28]

6.6 Discussion

The mathematical model formulation of the mechano-chemical coupling in single cardiomyocytes based on an active strain approach [51] has been analyzed and extended to realistic three-dimensional geometries. The proposed activation mechanism is consistent with a thermodynamic framework [55] entailing a nonlinear coupling among calcium dynamics and local stretches. The continuum approach adopted is on the line of recent bio-chemo-mechanical models of single cells [10, 11, 49] here formulated in terms of active-strain hyperelasticity. The model is capable to reproduce the propagation of calcium waves and the corresponding spontaneous contraction interacting within the cell [59], as well as the bending behavior, peculiar features of a three-dimensional structure. A finite element method is used to discretize the model equations; a set of numerical experiments comparing two- and three-dimensional reconstructed cardiomyocyte geometries give evidence of the main features of the model and its ability in predicting calcium propagation patterns and contractility in good agreement with experimental observations. Different boundary conditions have been analyzed reproducing physiological constraints thus analyzing the resulting stress patterns.

Limitations to the present study deal in particular with the correct treatment of boundary conditions in order to obtain physiological displacements of the cell. For the chemo-mechanic approach here discussed, numerical simulations show that Robin boundary conditions are better suited to reproduce the experimental observations even though a finer tuning of the Robin coefficients would be necessary. In this perspective an effective alternative would consider a level-set approach [31], in which an Eulerian description of the fluid-structure interaction problem considers the extracellular fluid interacting with the elastic cell via a *fictitious* interface. A careful representation of the internal cell anisotropy is equally fundamental due to the highly nonlinear coupling involved in the problem. In particular, intracellular micro-

structures, i.e. intercalated discs, should be taken into account for a more accurate geometric model. However, the lack of specific mechanical properties knowledge requires the usage of simplified cellular models. Therefore, the mathematical problem here addressed represents a good compromise in terms of continuum mechanics theory.

More realistic boundary conditions should be introduced also in terms of ionic exchanges other than calcium, i.e. Na and K [46]. The specific role of gap junctions and stretch-activated channel [52], discarded in the present study, can be addressed extending the numerical simulations to patch of cardiac tissue in a full multiscale approach characterized by a complete electromechanical coupling [66]. In this perspective, a more accurate modeling of the complex intracellular and extracellular calcium dynamics itself (Sodium-Calcium Exchanger and the NCX-NKA system [48]) would be considered for the analysis of rate-dependent effects, i.e. the positive force-frequency staircase effects [26, 35].

Extending the present formulation upon the discussed limitations would give insights and simulation-based predictions both for physiological [41] and pathological conditions [65] (failing myocardium conditions). We foresee the application of our model in describing the intra- and inter-cellular organization and remodeling of the myocyte structures during contraction [30] and the description of the diastolic calcium homeostasis as well [35]. Besides, our modeling approach can be extended to nonlocal constitutive laws mimicking micro-structure cellular adaptation to the external substrate [40]. It is tunable for cell biomechanics measurements tools and could be used as a framework to design and interpret novel experimental settings. We finally stress that the present model could be adopted as a building block in view of a multiscale cardiac model integrating cell, tissue and organ levels. Particular interest for the role of mechano-electric feedback in vulnerability to electric shocks [34] and in tissue pinning phenomena associated with arrhythmias [7, 47] is implied.

Acknowledgements We acknowledge the financial support by the European Research Council through the Advanced Grant *Mathcard, Mathematical Modelling and Simulation of the Cardiovascular System*, Project 227058, the International Center for Relativistic Astrophysics Network (ICRANet) and the Young Researcher Grant of the Italian Gruppo Nazionale per la Fisica Matematica (GNFM, INdAM).

References

1. Berry, M.F., Engler, A.J., Woo, Y.J., Pirolli, T.J., Bish, L.T., Jayasankar, V., Morine, K.J., Gardner, T.J., Discher, D.E., Sweeney, H.L.: Mesenchymal stem cell injection after myocardial infarction improves myocardial compliance. Am. J. Physio. Heart. Circ. Physiol. **290**, H2196–2203 (2006)
2. Bers, D.M.: Cardiac excitation–contraction coupling. Nature **415**, 198–205 (2002)
3. Bloom, S.: Spontaneous rhythmic contraction of separated heart muscle cells. Science **167**(3926), 1727–1729 (1970)
4. Cherry, E.M., Fenton, F.H.: Visualization of spiral and scroll waves in simulated and experimental cardiac tissue. New J. Phys. **10**, 125016 (2008)

5. Bueno-Orovio, A., Cherry, E.M., Fenton, F.H.: Minimal model for human ventricular action potentials in tissue. J. Theor. Biol. **253**, 544–560 (2008)
6. Capogrossi, M.C., Suarez-Isla, B.A., Lakatta, E.G.: The interaction of electrically stimulated twitches and spontaneous contractile waves in single cardiac myocytes. J. Gen. Physiol., **88**, 615–633 (1986)
7. Cherubini, C., Filippi, S., Gizzi, A.: Electroelastic unpinning of rotating vortices in biological excitable media. Phys. Rev. E, **85**, 031915 (2012)
8. Cherubini, C., Filippi, S., Nardinocchi, P., Teresi, L.: An electromechanical model of cardiac tissue: Constitutive issues and electrophysiological effects.Prog. Biophys. Mol. Biol., **97**, 562–573 (2008)
9. Delbridge, L.M.D., Roos, K.P.: Optical methods to evaluate the contractile function of unloaded isolated cardiac myocytes. J. Molec. Cell Cardiol., **29**, 11–25 (1997)
10. Deshpande, V.S., McMeeking, R.M., Evans, A.G.: A bio-chemo-mechanical model for cell contractility, PNAS, **103**, 14015–14020 (2006)
11. Deshpande, V.S., Mrksich, M., McMeeking, R.M., Evans, A.G.: A bio-mechanical model for coupling cell contractility with focal adhesion formation, J. Mech. Phys. Sol., **56**, 1484–1510 (2008)
12. Fabiato, A.: Appraisal of the physiological relevance of two hypothesis for the mechanism of calcium release from the mammalian cardiac sarcoplasmic reticulum: calcium-induced release versus charge-coupled release, Mol. Cell. Biochem., **89**, 135–140 (1989).
13. Fabiato, A., Fabiato, F.: Contractions induced by a calcium-triggered release of calcium from the sarcoplasmic reticulum of single skinned cardiac cells. J. Physiol. **249**(3), 469–495 (1975)
14. Fenton, F.H., Cherry, E.M.: Models of cardiac cells, Scholarpedia **3**, 1868 (2008)
15. Fenton, F.H., Gizzi, A., Cherubini, C., Pomella, N., Filippi, S.: Role of temperature on nonlinear cardiac dynamics, Phys. Rev. E Stat. Nonlin. Soft. Matter. Phys., **87**, 042709 (2013)
16. Geuzaine, C., Remacle, J.F.: Gmsh: a three-dimensional finite element mesh generator with built-in pre- and post-processing facilities. Int. J. Numer. Meth. Engrg., **79**, 1309–1331 (2009)
17. Gizzi, A., Cherubini, C., Filippi, S., Pandolfi, A.: Theoretical and Numerical Modeling of Nonlinear Electromechanics with applications to Biological Active Media, Commun. Comput. Phys. **17**(1), 93–126 (2015)
18. Göktepe, S., Abilez, O.J., Kuhl, E.: A generic approach towards finite growth with examples of athletes heart, cardiac dilation, and cardiac wall thickening. J. Mech. Phys. Sol., **58**, 1661–1680 (2010)
19. Goldbeter, A., Dupont, G., Berridge, M.J.: Minimal model for signal-induced Ca^{2+} oscillations and for their frequency encoding through protein phosphorylation. Proc. Natl. Acad. Sci. USA, **87**, 1461–1465 (1990)
20. Goldmann, W.H. Mechanotransduction in cells. Cell. Biol. Int. **36**, 567–70 (2012)
21. Grosberg, A., Kuo, P.L., Guo, C.L., Geisse, N.A., Bray, M.A., Adams, W.J., Sheehy, S.P., Parker, K.K.: Self-organization of muscle cell structure and function. PLoS Comp. Biol., **7**, e1001088 (2011)
22. Hatano, A., Okada, J., Washio, T., Hisada, T., Sugiura, S.: A three-dimensional simulation model of cardiomyocyte integrating excitation-contraction coupling and metabolism. Biophys. J., **101**, 2601–2610 (2011)
23. Holzapfel, G.A., Ogden, R.W.: Constitutive modelling of passive myocardium: a structurally based framework for material characterization. Phil. Trans. R. Soc. Lond. A, **367**, 3445–3475 (2009)

24. Humphrey, J.D.: Stress, strain, and mechanotransduction in cells. J. Biomech. Eng. **123**, 638–641 (2001)
25. Iribe, G., Helmes, M., Kohl, P.: Force-length relations in isolated intact cardiomyocytes subjected to dynamic changes in mechanical load. Am. J. Physiol. Heart Circ. Physiol., **292**, H1487–H1497 (2007)
26. Iribe, G., Ward, C.W., Camelliti, P., Bollensdorff, C., Mason, F., Burton, R.A.B., Garny, A., Morphew, M., Hoenger, A., Lederer, W.J., Kohl, P.: Axial stretch of rat single ventricular cardiomyocytes causes an acute and transient increase in Ca^{2+} spark rate. Circ. Res., **104**, 787–795 (2009)
27. Iyer, V., Mazhari, R., Winslow, R.L.: A computational model of the human left ventricular epicardial myocyte. Biophys. J., **87**, 1507–1525 (2004)
28. Kamgoué, A., Ohayon, J., Usson, Y., Riou, L., Tracqui, P.: Quantification of cardiomyocyte contraction based on image correlation analysis. Cytometry Part A **75**, 298–308 (2009)
29. Keener, J., Sneyd, J.: Mathematical physiology, Springer-Verlag, New York (1998)
30. Kockskåmper, J., von Lewinski, D., Khafaga, M., Elgner, A., Grimm, M., Eschenhagen, T., Gottlieb, P.A., Sachs, F., Pieske, B.: The slow force response to stretch in atrial and ventricular myocardium from human heart: functional relevance and subcellular mechanisms. Prog. Biophys. Mol. Biol., **97**, 250–267 (2008)
31. Laadhari, A., Ruiz-Baier, R., Quarteroni, A.: Fully Eulerian finite element approximation of a fluid-structure interaction problem in cardiac cells. Int. J. Numer. Meth. Engrg., **96**, 712–738 (2013)
32. Lubarda, V.A.: Constitutive theories based on the multiplicative decomposition of deformation gradient: Thermoelasticity, elastoplasticity, and biomechanics. Appl. Mech. Rev., **57**, 95–108 (2004)
33. Li, J., Patel, V.V., Radice, G.L.: Dysregulation of cell adhesion proteins and cardiac arrhythmogenesis, Clin. Med. Res., **4**, 42–52 (2006)
34. Li, W., Gurev, V., McCulloch, A.D., Trayanova, N.A.: The role of mechanoelectric feedback in vulnerability to electric shock, Prog. Biophys. Mol. Biol., **97**, 461–478 (2008)
35. Louch, W.E., Stokke, M.K., Sjaastad, I., Christensen, G., Sejersted, O.M.: No rest for the weary: diastolic calcium homeostasis in the normal and failing myocardium, Physiology, **27**, 308–323 (2008)
36. Marshall, K.L., Lumpkin, E.A.: The molecular basis of mechanosensory transduction. Adv. Exp. Med. Biol., **739**, 142–55 (2012)
37. McCain, M.L., Lee, H.L., Aratyn-Schaus, Y., Kléber, A.G., Parker, K.K. Cooperative coupling of cell-matrix and cell-cell adhesions in cardiac muscle. PNAS, **109**, 9881–9886 (2012)
38. Nardinocchi, P., Teresi, L.: Electromechanical modeling of anisotropic cardiac tissues. Math. Mech. Solids, **18**, 576–591 (2013)
39. Nobile, F., Quarteroni, A., Ruiz-Baier, R.: An active strain electromechanical model for cardiac tissue. Int. J. Numer. Meth. Biomed. Engrg., **28**, 52–71 (2012)
40. Novak, I.L., Slepchenko, B.M., Mogilner, A., Loew, L.M.: Cooperativity between cell contractility and adhesion. Phys. Rev. Lett., **93**, 268109 (2004)
41. Nishimura, S., Seo, K., Nagasaki, M., Hosoya, Y., Yamashita, H., Fujita, H., Nagai, R., Sugiura, S.: Responses of single-ventricular myocytesto dynamic axial stretching. Prog. Biophys. Mol. Biol., **97**, 282–297 (2008)
42. Ortiz, M., Stainier, L.: The variational formulation of viscoplastic constitutive updates. Comp. Meth. Appl. Mech. Eng., **171**, 419–444 (1999)

43. Ortiz, M., Pandolfi, A.: A variational Cam-clay theory of plasticity. Comp. Meth. Appl. Mech. Eng., **193**, 2645–2666 (2004).
44. Pandolfi, A., Conti, S., Ortiz, M.: A recursive-faulting model of distributed damage in confined brittle materials. J. Mech. Phys. Sol., **54**, 1972–2003 (2006)
45. Parker, K.K., Tan, J., Chen, C.S., Tung, L.: Myofibrillar architecture in engineered cardiac myocytes. Circ. Res., **103**, 340–342 (2008)
46. Pullan, A.J., Buist, M.L., Cheng, L.K.: Mathematically Modeling the Electrical Activity of the Heart: From Cell to Body Surface and Back, World Scientific, Singapore (2005)
47. Pumir, A., Sinha, S., Sridhar, S., Argentina, M., Horning, M., Filippi, S., Cherubini, C., Luther, S., Krinsky, V.: Wave-train-induced termination of weakly anchored vortices in excitable media. Phys. Rev. E, **82**, 010901(R) (2010)
48. Rice, J.J., Wang, F., Bers, D.M., de Tombe, P.P. Approximate model of cooperative activation and crossbridge cycling in cardiac muscle using ordinary differential equations. Biophys. J., **95**, 2368–2390 (2008)
49. Ronan, W., Deshpande, V.S., McMeeking, R.M., McGarry, J.P.: Numerical investigation of the active role of the actin cytoskeleton in the compression resistance of cells. J. Mech. Behav. Biomed. Mat., **14**, 143–157 (2012)
50. Rossi, S., Lassila, T., Ruiz-Baier, R., Sequeira, A., Quarteroni, A.: Thermodynamically consistent orthotropic activation model capturing ventricular systolic wall thickening in cardiac electromechanics. Eur. J. Mech. A/Solids **48**, 129–142 (2014)
51. Ruiz-Baier, R., Gizzi, A., Rossi, S., Cherubini, C., Laadhari, A., Filippi, S., Quarteroni, A.: Mathematical modelling of active contraction in isolated cardiomyocytes, Math. Med. Biol. **31**, 259–283 (2014)
52. Seol, C.A., Kim, W.T., Ha, J.M., Choe, H., Jang, Y.J., Youm, J.B., Earm, Y.E., Leem, C.H.: Stretch-activated currents in cardiomyocytes isolated from rabbit pulmonary veins. Prog. Biophys. Mol. Biol., **97**, 217–231 (2008)
53. Sheehy, S.P., Grosberg, A., Parker, K.K.: The contribution of cellular mechanotransduction to cardiomyocyte form and function. Biomech. Model. Mechanobiol. **11**, 1227–1239 (2012)
54. Sneyd, J., Ed.: Tutorials in Mathematical Biosciences II: Mathematical Modeling of Calcium Dynamics and Signal Transduction, Springer, ISBN 978-3-540-25439-3 (2005)
55. Stålhand, J., Klarbring, A., Holzapfel, G.A.: A mechanochemical 3D continuum model for smooth muscle contraction under finite strains. J. Theoret. Biol., **268**, 120–130 (2011).
56. Stern, M.D.: Theory of excitation-contraction coupling in cardiac muscle. Biophys. J., **63**, 497–517 (1992)
57. Subramanian, S., Viatchenko-Karpinski, S., Lukyanenko, V., Györk, S., Wiesner, T.F. Underlying mechanisms of symmetric calcium wave propagation in rat ventricular myocytes. Biophys. J., **80**, 1–11 (2001)
58. Taber, L.A.: Biomechanics of cardiovascular development. Annu. Rev. Biomed. Eng., **3**, 1–25 (2001)
59. Takamatsu, T., Wier, W.G.: Calcium waves in mammalian heart: quantification of origin, magnitude, waveform and velocity. Fed. Am. Soc. Exp. Biol., **4**, 1519–1525 (1990)
60. Ter Keurs, H.E.D.J., Boyden, P.A.: Calcium and arrhythmogenesis. Physiol. Rev. **87**(2), 457–506 (2007)
61. Tracqui, P., Ohayon, J.: An integrated formulation of anisotropic force-calcium relations driving spatio-temporal contractions of cardiac myocytes. Phil. Trans. Royal Soc. London A, **367**, 4887–4905 (2009)

62. Tveito, A., Lines, G.T., Edwards, A.G., Maleckar, M.M., Michailova, A., Hake, J., McCulloch, A.D.: Slow Calcium-Depolarization-Calcium waves may initiate fast local depolarization waves in ventricular tissue. Prog. Biophys. Molec. Biol., **110**, 295–304 (2012)
63. Vogel, F., Bustamante, R., Steinmann, P.: On some mixed variational principles in electro-elastostatics. Int. J. Nonlin. Mech., **47**, 341–354 (2012)
64. Washio, T., Okada, J. Sugiura, S., Hisada, T.: Approximation for cooperative interactions of a spatially-detailed cardiac sarcomere model. Cell. Mol. Bioeng., **5**, 113–126 (2012)
65. Ward, M.L., Williams, I.A., Chu, Y., Cooper, P.J., Ju, Y.K., Allen, D.G.: Stretch-activated channels in the heart: contributions to length-dependence and to cardiomyopathy.Prog. Biophys. Mol. Biol., **97**, 232–249 (2008)
66. Zhang, Y., Sekar, R.B., McCulloch, A.D., Tung, L.: Cell cultures as models of cardiac mechanoelectric feedback. Prog. Biophys. Mol. Biol., **97**, 367–382 (2008)